LEVEL II

DCW INDUSTRIES

13535 VENTURA BLVD., SUITE 207, SHERMAN OAKS, CALIF. 91423

(9) Interim rept. 1 apr - 30 jul 75

(1)

(18) (19)

AFOSR-TR-75-1398

(14) DCW-R-03-03

(6)

EFFECTS OF SURFACE HEAT TRANSFER ON BOUNDARY-LAYER TRANSITION

by Thom as

(10) David D.C. Wilcox and T.L. Chambers

(11) July 1975

(12) 38

Prepared for

AIR FORCE OFFICE OF SCIENTIFIC RESEARCH/NA
Arlington, Virginia 22209

(16) 9781

(17) 02

Sponsored by

ADVANCED RESEARCH PROJECTS AGENCY
ARPA Order No. 2980

(15)

Contract No.: F44620-74-C-0048 (P00003)
Amount of Contract: $15,609.00
Program Code: 5G10
Effective Date of Contract: April 1, 1975
Contract Expiration Date: July 30, 1975

Principal Investigator/Program Manager:

David C. Wilcox,
(213) 990-2682

DCW Industries
13535 Ventura Boulevard, Suite 207
Sherman Oaks, California 91423
(213) 990-2682

391224

15

ABSTRACT

Effects of surface heat transfer on boundary-layer transition are analyzed in a three-part study using the Saffman-Wilcox transition model. In the first part of the study, model predictions are compared with experimental data for cooled and heated aerodynamic boundary layers on smooth flat surfaces and for cooled aerodynamic boundary layers near the stagnation point of a roughened blunt body. Consistent with measurements, the model predicts, on the one hand, that heating destabilizes a smooth-surface aerodynamic boundary layer and, on the other hand, that cooling destabilizes a rough-surface aerodynamic boundary layer. Differences between predicted and measured transition-point locations are within experimental error bounds. Then, incipient transition conditions are determined for a small, heated hydrodynamic body. Again model predictions agree with measurements which indicate that relatively small amounts of surface heating have a strong stabilizing effect on hydrodynamic boundary layers. In the final part of the study, transition location is determined for a large hydrodynamic body; results indicate that large surface heating rates are not substantially more effective than smaller rates.

CONTENTS

SECTION		PAGE
	ABSTRACT	ii
	CONTENTS	iii
	NOTATION	iv
1.	INTRODUCTION	1
2.	FORMULATION	3
	2.1 Equations of Motion	3
	2.2 Neutral Stability Considerations	6
3.	APPLICATIONS	10
	3.1 Heated and Cooled Aerodynamic Boundary Layers	10
	3.2 Heated Hydrodynamic Boundary Layers on Small Bodies	14
	3.3 Heated Hydrodynamic Boundary Layers on Large Bodies	19
4.	SUMMARY AND CONCLUSIONS	23
	APPENDIX A: THERMODYNAMIC PROPERTIES OF WATER	24
	APPENDIX B: HYDRODYNAMIC BODY SHAPE PARAMETERS	26
	REFERENCES	27

NOTATION

SYMBOL	DEFINITION
c_p	Pressure coefficient, $(p-p_\infty)/(1/2\rho U_\infty^2)$
C_p	Specific heat at constant pressure
e	Specific turbulent energy
f_r	Parsons-Goodson-Goldschmied shape parameter
$F(\eta)$	Nondimensional self-similar velocity profile
j	0 for two-dimensional flow; 1 for axisymmetric flow
k	Roughness height
k_i	Parsons-Goodson-Goldschmied shape parameter
p	Pressure
Pr_L, Pr_T	Laminar and turbulent Prandtl numbers
q_w, $\bar{q}_w$	Surface heating rate; average value of q_w
r	Radial distance from symmetry axis
r_i, r_n	Parson-Goodson-Goldschmied shape parameters
R_o	Empirical constant
Re_s, Re_x	Reynolds number based on arclength, plate length
Re_θ	Reynolds number based on momentum thickness
Re_V	Incipient transition Reynolds number based on $V^{1/3}$
s	Arclength
s_i	Parsons-Goodson-Goldschmied shape parameter
t	Parsons-Goodson-Goldschmied shape parameter
T	Temperature
T_{t_∞}	Freestream total temperature
T'_∞	Freestream turbulence intensity
u,v	Velocity component in x,y direction
U_e	Boundary-layer-edge velocity
U_∞	Freestream velocity
V	Body volume

NOTATION (cont.)

SYMBOL	DEFINITION
x,y	Distance parallel to, normal to body surface
x_m, x_i	Parsons-Goodson-Goldschmied shape parameter
α, α^*	Empirical parameters
β, β^*	Empirical constants
η	Similarity variable
θ	Momentum thickness
κ	Karman's constant; thermal conductivity
λ, λ^*	Empirical parameters
Λ	Modified Polhausen pressure gradient parameter
μ	Molecular viscosity
ν	Kinematic viscosity
ρ	Fluid density
σ, σ^*	Empirical constants
Ω	Specific dissipation rate

Subscripts

e	Boundary layer edge
t	Transition point
w	Surface
∞	Freestream

1. INTRODUCTION

In recent years, substantial progress has been made toward maintaining laminar flow, and hence low drag, over aerodynamic/hydrodynamic bodies at practical flow speeds. In the case of aerodynamic bodies, the use of carefully designed airfoil shapes (e.g. to provide strong favorable pressure gradient) and the use of boundary-layer-control techniques (e.g. suction) has successfully delayed transition to chord-length Reynolds numbers, Re_{s_t}, of the order of 10 million. Even larger values of Re_{s_t} have been achieved for small hydrodynamic bodies through the use of surface heating and pressure gradient. For hydrodynamic bodies, extrapolations based on linear stability theory indicate that, with practicable amounts of surface heating, values of Re_{s_t} in excess of 200 million may be possible on relatively large hydrodynamic bodies[1].

The reduction in drag which can be achieved by maintaining laminar flow over <u>any</u> vehicle is attractive because of the reduced power requirements to move the vehicle. However, a penalty is generally paid in maintaining laminar flow on <u>lifting</u> bodies in that a laminar boundary layer separates much more easily than does a turbulent boundary layer, resulting in a significant reduction in lift. Hence, maintaining laminar flow is practical mainly for <u>nonlifting</u> bodies. Submarines and torpedos or, more generally, hydrodynamic bodies fall into the latter class.

This study focuses on the observed pronounced effects of surface heat transfer on boundary layer transition. Most importantly, this report includes transition predictions based on a relatively new transition theory for small and large heated hydrodynamic bodies.

Section 2 presents the transition equations, including a modification needed to improve transition-prediction accuracy when surface heat transfer is present. Included in Section 3 are transition computations for various aerodynamic and hydrodynamic boundary layers. The concluding section summarizes results and conclusions.

2. FORMULATION

2.1 EQUATIONS OF MOTION

The Saffman-Wilcox transition model[2-4] is the basic tool used in this study to analyze effects of surface heat transfer on boundary-layer transition. The model's accuracy has previously been demonstrated for a wide variety of flows ranging from incompressible boundary layers to hypersonic blunt-body flows. These applications have tested the model's ability to predict transition sensitivity to effects of free-stream turbulence, suction, surface roughness and pressure gradient. In all cases, accuracy acceptable for most engineering purposes has been obtained.

For incompressible boundary layers (i.e., for very small Mach numbers), the equations of motion which constitute the transition model are:

Mass Conservation

$$\frac{\partial}{\partial x}(r^j u) + \frac{\partial}{\partial y}(r^j v) = 0 \tag{1}$$

Momentum Conservation

$$\rho u \frac{\partial u}{\partial x} + \rho v \frac{\partial u}{\partial y} = -\frac{dp}{dx} + \frac{1}{r^j}\frac{\partial}{\partial y}\left[r^j(\mu + \frac{e}{\Omega})\frac{\partial u}{\partial y}\right] \tag{2}$$

Energy Conservation

$$\rho u \frac{\partial(C_p T)}{\partial x} + \rho v \frac{\partial(C_p T)}{\partial y} = u\frac{dp}{dx} + \frac{1}{r^j}\frac{\partial}{\partial y}\left[r^j\left(\frac{\mu}{Pr_L} + \frac{e/\Omega}{Pr_T}\right)\frac{\partial(C_p T)}{\partial y}\right] \tag{3}$$

Turbulent Energy

$$\rho u \frac{\partial e}{\partial x} + \rho v \frac{\partial e}{\partial y} = \left[\alpha^* \left|\frac{\partial u}{\partial y}\right| - \beta^* \rho \Omega\right] \rho e + \frac{1}{r^j} \frac{\partial}{\partial y}\left[r^j (\mu + \sigma^* \frac{e}{\Omega}) \frac{\partial e}{\partial y}\right] \quad (4)$$

Turbulent Dissipation Rate

$$\rho u \frac{\partial \Omega^2}{\partial x} + \rho v \frac{\partial \Omega^2}{\partial y} = \left[\alpha \left|\frac{\partial u}{\partial y}\right| - \beta \rho \Omega\right] \rho \Omega^2 + \frac{1}{r^j} \frac{\partial}{\partial y}\left[r^j (\mu + \sigma \frac{e}{\Omega}) \frac{\partial \Omega^2}{\partial y}\right] \quad (5)$$

In Equations 1-5, x and y are orthogonal coordinates parallel to and normal to a body surface. The quantity r is the radial coordinate from the body's symmetry axis while j=0 for two dimensional flow and j=1 for axisymmetric flow. The velocity components in the x and y directions are denoted by u and v; fluid density, temperature, pressure, specific heat, and viscosity are denoted by ρ, T, p, C_p, and μ respectively. The quantities e and Ω are specific turbulent energy and specific turbulent dissipation rate; their ratio, e/Ω, is the turbulent eddy viscosity.

Both air and water are considered in this study. The various thermodynamic properties for air are related through the perfect gas law and the Sutherland viscosity law. Appendix A lists the pertinent thermodynamic properties of water.

Several empirical parameters appear in Equations 1-5. For transitional flows, past studies[2-4] have established the following values:

$$\left.\begin{array}{c} Pr_T = 0.89 \\ \beta = 0.15 \quad , \quad \beta^* = 0.09 \\ \sigma = 0.50 \quad , \quad \sigma^* = 0.50 \end{array}\right\} \quad (6)$$

$$\alpha^* = 0.30 \left[1 - (1 - \lambda^*)(1 - Re_T/R_o)\, H\,(1 - Re_T/R_o)\right] \qquad (7)$$

$$\alpha = .1638 \left[1 - (1 - \lambda)(1 - Re_T/R_o)\, H\,(1 - Re_T/R_o)\right] \qquad (8)$$

where $H(x)$ is the Heaviside stepfunction and Re_T is turbulent Reynolds number defined by

$$Re_T = e/\Omega\mu \qquad (9)$$

Finally, the parameters λ^* and R_o are constants whose values are

$$\lambda^* = 0.105 \ , \ R_o = 0.10 \qquad (10)$$

The quantity λ depends upon the freestream turbulence level, T', and pressure gradient parameter, Λ, defined by

$$T' = 100 \sqrt{\frac{2}{3} \frac{e_e}{U_e^2}} \qquad (11)$$

and

$$\Lambda = \frac{\rho_e}{\rho_w} \frac{\theta^2}{\nu_e} \frac{dU_e}{dx} \qquad (12)$$

The functional dependence of λ upon Λ and T' is

$$\lambda = .105\left(1 + 2H(\Lambda) \left\{1 - \exp\left[-40\Lambda\right]\right\} \exp\left[-3T'^2\right]\right) \qquad (13)$$

Equations 1-3 are the time-averaged conservation equations with classical eddy-viscosity and eddy-heat-diffusivity closure approximations. Equations 4 and 5 are nonlinear diffusion equations for e and Ω which provide a description of the growth

of disturbances in a laminar flow up to, through, and beyond transition. Wilcox[2] presents a thorough discussion of the way in which the model equations are used to predict boundary-layer transition. Boundary conditions suitable for flow over both smooth and rough surfaces are given by Wilcox and Chambers[4].

2.2 NEUTRAL STABILITY CONSIDERATIONS

Qualitative features of model-predicted transition can be conveniently determined by dropping the convection and diffusion terms in the turbulent-energy equation (Equation 4). In doing this we can determine the neutral-stability point which is defined as the point in a boundary layer where turbulent energy generation, $\alpha^* \rho e |\partial u/\partial y|$, just balances turbulent energy dissipation, $\beta^* \rho^2 \Omega e$. Hence, neutral stability is defined by the following condition:

$$\max_y \frac{\alpha^*}{\beta^*} \frac{|\partial u/\partial y|}{\rho \Omega} = 1 \tag{14}$$

Then, noting for laminar boundary layers that Ω and α^* are approximately[2]

$$\Omega \doteq \frac{20}{\beta} \frac{\mu}{\rho^2 y^2} \tag{15}$$

$$\alpha^* \doteq 0.30 \lambda^* \tag{16}$$

Equation 14 simplifies to

$$\max_y \frac{y^2}{\nu} \left|\frac{\partial u}{\partial y}\right| = \frac{40}{\lambda^*} \tag{17}$$

For zero-pressure-gradient boundary layers in air, the velocity distribution can be written as

$$u = U_e F(\eta) \tag{18}$$

where

$$\eta \equiv y\sqrt{\frac{U_e}{\nu_w x}} \tag{19}$$

Using Equations 18 and 19, Equation 17 simplifies to the following:

$$\sqrt{\frac{U_e x}{\nu_w}} = \frac{40/\lambda^*}{\max_\eta \eta^2 \left|\frac{\partial F}{\partial \eta}\right|} \tag{20}$$

Now for incompressible flow, $F(\eta)$ is only weakly dependent upon surface heat transfer. Hence, Equation 20 implies that the neutral stability Reynolds number, $U_e x/\nu_w$, varies inversely as λ^{*2}. Experiments[5] indicate that transition Reynolds number, $U_e x_t/\nu_w$, is inversely proportional to $(T_w/T_e)^2$. Assuming that the transition Reynolds number is proportional to the neutral stability Reynolds number (as it often is) implies that λ^* should be proportional to T_w/T_e.

Computations with λ^* independent of T_w/T_e verified that such a dependence is needed. The unmodified model predicted that heating (cooling) has a stabilizing (destabilizing) effect on aerodynamic boundary layers, in contrast to the measured destabilizing (stabilizing) effect. These predictions were unsurprising as Shamroth and McDonald[5] find a similar reversal in predicted transition sensitivity to heating and cooling with their turbulence-model transition method. Shamroth and McDonald resolve the problem by making a parameter similar to

λ^* an increasing function of T_w/T_e. While this model revision is sufficient to yield accurate transition location for aerodynamic boundary layers, it is inadequate for the hydrodynamic case. That is, according to Equation 20, transition location, x_t, is proportional to μ_w/λ^{*2}. For a liquid, μ_w varies as T_w^{-8} near room temperature (see Appendix A. Hence, assuming λ^* is proportional to T_w would imply that x_t varies as T_w^{-10}. Therefore, increasing surface temperature would decrease x_t, i.e., heating would destabilize a hydrodynamic boundary layer. Since heating stabilizes such a boundary layer, a different modification is clearly needed.

The parameter λ^* should more appropriately depend upon μ_w/μ_e. On the one hand, μ_w/μ_e increases as T_w/T_e increases for air, while, on the other hand, μ_w/μ_e decreases as T_w/T_e increases for water. Thus, if λ^* were proportional to some power of μ_w/μ_e, the model could accurately predict effects of surface heat transfer on both aerodynamic and hydrodynamic boundary layer transition. Since $\mu \sim T^{3/4}$ for air, the following revised form of Equation 20 is proposed:

$$\lambda^* = 0.105\ (\mu_w/\mu_e)^{4/3} \tag{10a}$$

An additional, less obvious, modification is needed. Note that the parameter λ partially controls the rate at which disturbances are amplified beyond the neutral stability point. Furthermore, if λ ever becomes sufficiently large (relative to λ^*) so that dissipation-rate production, $\alpha\rho\Omega^2|\partial u/\partial y|$, overtakes dissipation-rate dissipation, $\beta\rho^2\Omega^3$, (see Equation 5) before the neutral stability point is reached, transition may never occur. Thus, if λ remains

unaltered, the possibility exists that a finite amount of cooling (heating) will cause an aerodynamic (hydrodynamic) boundary layer to forever remain laminar, a physically unrealistic prediction. Hence, Equation 13 must be replaced by:

$$\lambda = .105(\mu_w/\mu_e)^{4/3}\left\{1 + 2H(\Lambda)[1 - \exp(-40\Lambda)]\exp(-3T'^2)\right\} \qquad (13a)$$

All of the computations presented in the next section have been performed using the transition model defined by Equations 1 through 9, 10a, 11, 12, and 13a; as noted earlier, appropriate surface boundary conditions are given by Wilcox and Chambers[4].

3. APPLICATIONS

In the first part of this section, the transition model is used to predict transition sensitivity to surface heat transfer for smooth- and rough-surface aerodynamic boundary layers; computed transition-point locations are compared with corresponding experimental data. Then, effects of surface heating on a small hydrodynamic body are computed; qualitative comparisons are made with experimental data. Finally, transition location is predicted on a large hydrodynamic body.

3.1 HEATED AND COOLED AERODYNAMIC BOUNDARY LAYERS

One of the easiest of all flows to analyze is the incompressible flat-plate boundary layer (FPBL). Furthermore, analyzing this flow provides a good test of the transition model as detailed measurements have been made[6] to determine transition sensitivity to surface heat transfer. Using an incompressible version of DCW Industries' EDDYBL computer code[2], transition computations were performed for an incompressible FPBL with

$$0.5 \leq T_w/T_e \leq 3.0 \tag{21}$$

As in all computations in this study, the value of Ω at the boundary-layer edge, Ω_e, was given by

$$\Omega_e = .0185U_e^2/\mu_e \tag{22}$$

a value generally used in EDDYBL transition calculations. Results of the computations are shown in Figure 1; experimental

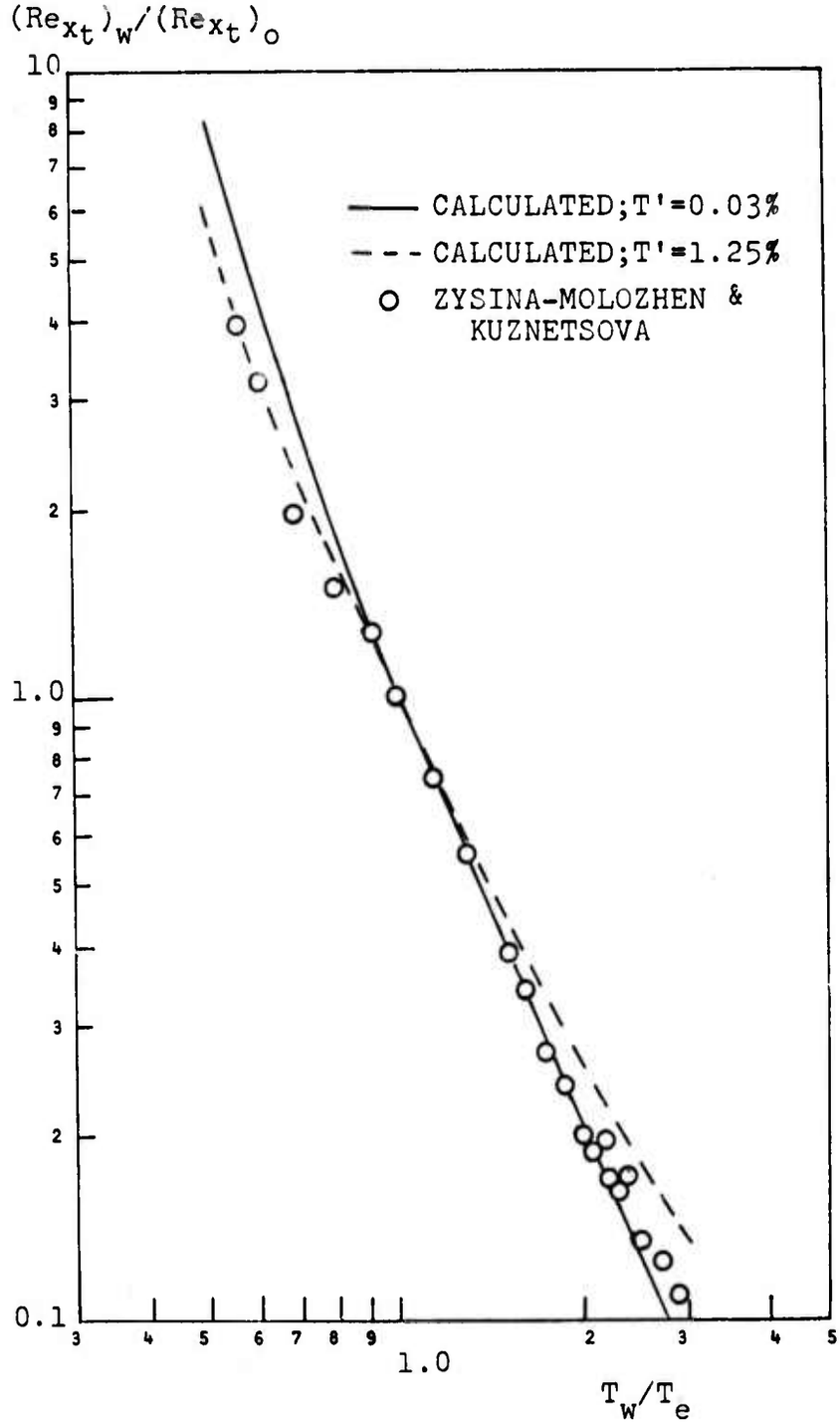

Figure 1. Computed and measured effects of surface heating and cooling on boundary layer transition in air; $(Re_{x_t})_w$ = plate-length transition Reynolds number based on surface conditions; $(Re_{x_t})_o$ = the value of Re_{x_t} without surface heat transfer.

data of Zysina-Molozhen and Kuznetsova[6] are included in the figure for comparison.

Because the freestream turbulence level in the experiments was not available, computations were done for a relatively high level (T'=1.25%) and for a relatively low level (T'=.03%). As shown in the figure, freestream turbulence level has only a slight effect on transition Reynolds number based on surface conditions, $(Re_{x_t})_w \equiv U_e x_t/\nu_w$. Consistent with the measurements, computed $(Re_{x_t})_w$ is approximately inversely proportional to $(T_w/T_e)^2$; computed values of $(Re_{x_t})_w$ generally are within about 20% of corresponding measured values.

A second, more subtle, test of the theory is to apply the equations to rough-wall aerodynamic boundary layers. Surface cooling can actually reverse its stabilizing role to one of destabilization when the surface is rough. The explanation for this phenomenon is well understood. The destabilization occurs because cooling thins the boundary layer, thus making the roughness look larger relative to a boundary-layer thickness such as momentum thickness, θ. Hence, the surface looks rougher, whereby transition occurs earlier.

To test the model's ability to predict this phenomenon, computations were performed for Mach 5 airflow past a roughened spherical body with nose radius of 2.5 inches; roughness heights, k, between 1.5 mils and 10 mils were used in the computations. Freestream unit Reynolds number ranged from 3 to 10 million per foot. (The compressible version of the model equations[4] was used for these calculations). The ratio of surface temperature to freestream total temperature, T_{t_∞},

was varied from 0.2 to 0.8. Figure 2 compares results of the computations with a correlation of experimental data[7]. Consistent with the measured effect, momentum thickness Reynolds number at transition, Re_{θ_t}, increases with decreasing surface temperature.

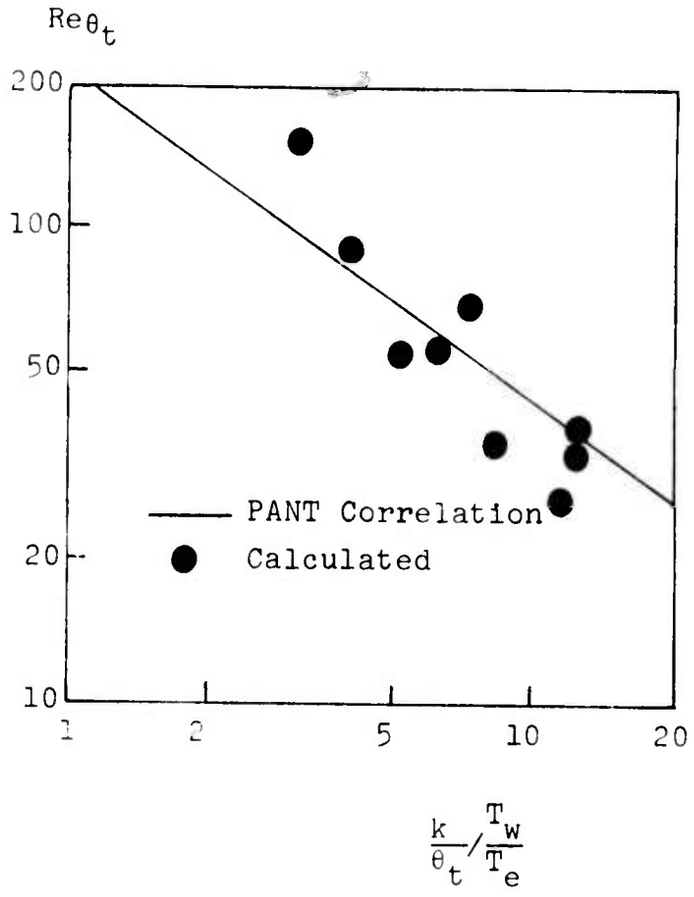

Figure 2. Comparison between computed and measured effects of surface cooling on rough-wall aerodynamic boundary-layer transition.

3.2 HEATED HYDRODYNAMIC BOUNDARY LAYERS ON SMALL BODIES

The second round of applications is to a small heated hydrodynamic body. The body, shown in Figure 3, is a Parsons-Goodson-Goldschmied[8] (PPG) minimum-drag hull shape which will be referred to as the H-2 body; the PPG body parameters are given in Appendix B. The objective of the computations was to determine incipient transition conditions for various surface temperatures. By definition, incipient transition occurs when the transition point is located at the maximum body radius.

All computations were performed with the following conditions specified:

Ambient Temperature, T_e	= 71°F
Roughness Height, k	= 16 μin
Freestream Turbulence, T'	= .01%
Freestream Dissipation Rate, Ω_e	= .0185 U_e^2/μ_e

The pressure distribution was obtained from the Douglas-Neumann[9] potential flow program; Figure 4 shows the computed pressure coefficient, c_p, defined by

$$c_p = (p-p_\infty)/(1/2\rho U_\infty^2) \qquad (23)$$

In the figure, z is axial distance from the stagnation point. Three series of computations were performed in which surface temperature was held constant at values of 71°F, 76°F, and 81°F. Incipient transition Reynolds number, Re_V (based on freestream flow conditions and $V^{1/3}$ where V is body volume), was computed for each value of T_w. Results of the calculations are summarized in Table 1; in addition to Re_V, the table gives freestream velocity, U_∞, transition Reynolds number based on

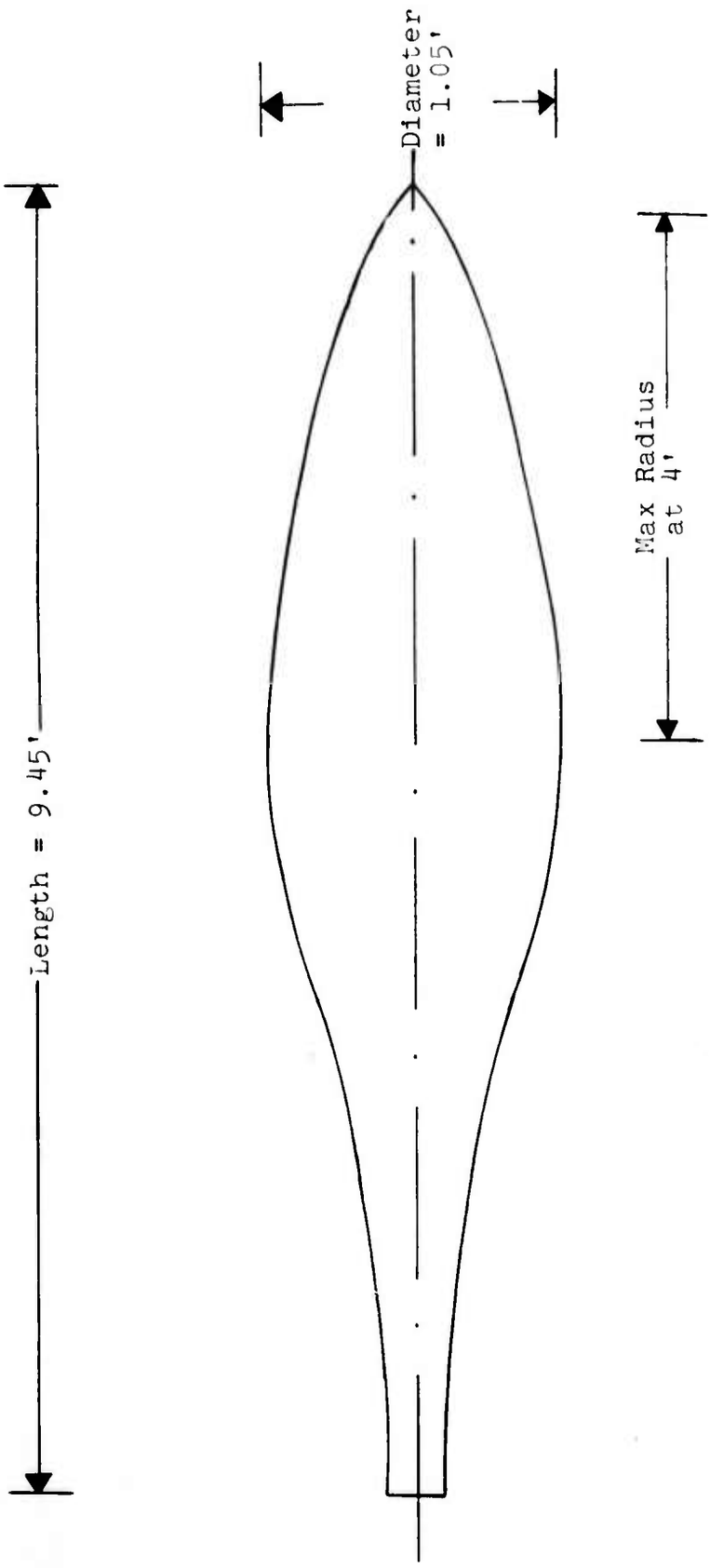

Figure 3. Hull shape for the small hydrodynamic body.

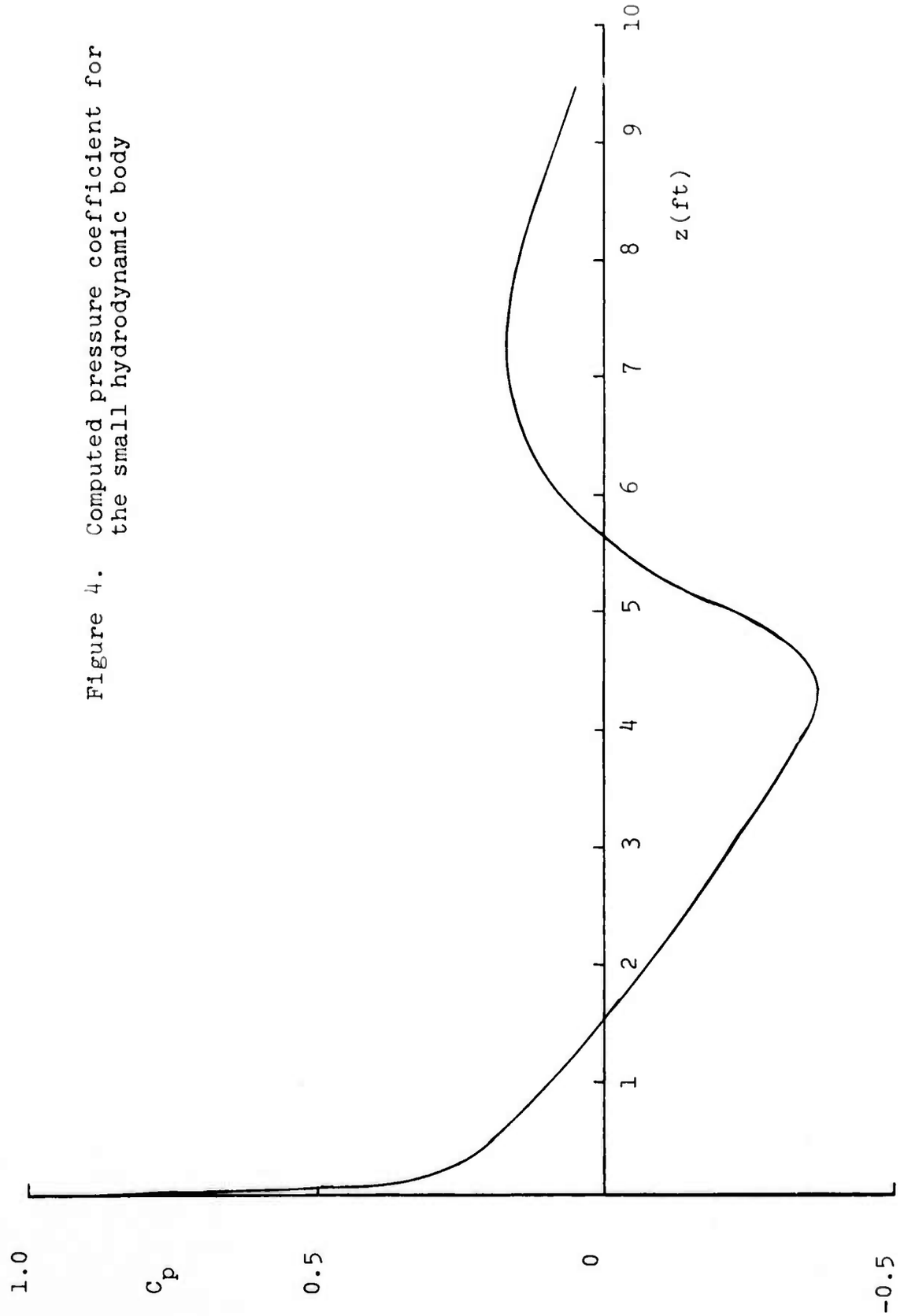

Figure 4. Computed pressure coefficient for the small hydrodynamic body

arclength, Re_{s_t}, and average heating rate, $\bar{q}_w$, defined by

$$\bar{q}_w = \frac{1}{s_t} \int_o^{s_t} q_w(s)\, ds \qquad (24)$$

In Equation 24, $s_t = 4$ feet (the maximum radius point), and $q_w(s)$ is the local heat transfer. Figure 5 shows computed Re_V as a function of $T_w - T_e$ and $\bar{q}_w$. As can be seen from the figure, heating stabilizes the boundary layer and hence increases the value of Re_V. This prediction is qualitatively consistent with the observed stabilizing effect of surface heating when the fluid is a liquid. The magnitude of the effect is also realistic[1].

Table 1. Computed Incipient Transition Conditions for the H-2 Body for Varying Surface Temperature.

$T_w - T_e$ (°F)	$\bar{q}_w$ ($\frac{kwatts}{ft^2}$)	U_∞ (knots)	$10^{-6} Re_V$	$10^{-6} Re_{s_t}$
0	0.00	25.3	9.4	18.2
5	0.31	35.0	13.0	24.5
10	1.30	47.4	17.6	33.8

An interesting feature of the predictions is revealed in Figure 5. Specifically, Re_V increases approximately linearly with $T_w - T_e$ for the range of temperatures considered. However, Re_V increases much less rapidly with $\bar{q}_w$. Hence, increasing the heating rate beyond about 2 kwatts/ft^2 may not yield substantial increases in Re_V.

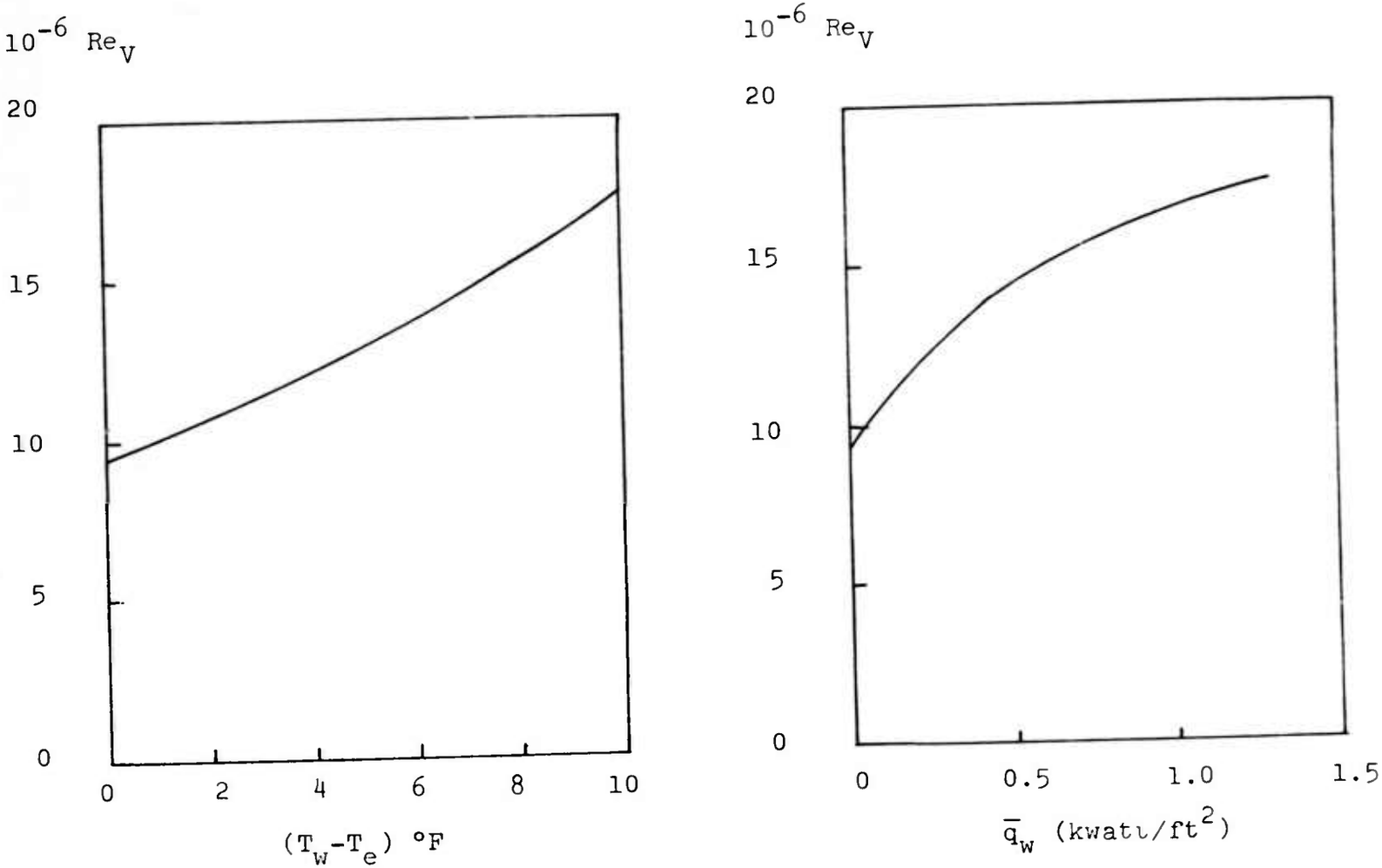

Figure 5. Computed incipient transition Reynolds number for the small hydrodynamic body.

3.3 HEATED HYDRODYNAMIC BOUNDARY LAYERS ON LARGE BODIES

The final application of the transition model is to a large heated hydrodynamic body. Again, a PPG hull shape, referred to as the R-9a body, is used (see Appendix B). The objective of these computations was to determine transition point location for specified flow conditions.

Two computations were performed; in one, the freestream flow speed, U_∞, was 35 knots and in the other U_∞ was 30 knots. In both computations, the following conditions were imposed:

Ambient Temperature, T_e	= 55°F
Surface Temperature, T_w	= 85°F
Roughness Height, k	= 16 μin
Freestream Turbulence, T'	= .01%
Freestream Dissipation Rate, Ω_e	= .0185 U_e^2/μ_e

Figure 6 shows the Douglas-Neumann-computed pressure distribution.

Table 2 and Figure 7 summarize results of the computations. For both flow speeds, transiton occurs well upstream of the maximum radius. Computed arclength transition Reynolds numbers, Re_{s_t}, are not much larger than the value achieved on the H-2 body with $\bar{q}_w$ = 1.30 kwatts/ft^2 (see Table 1). Noting the heating rates involved, the predictions are consistent with results of the preceding subsection.

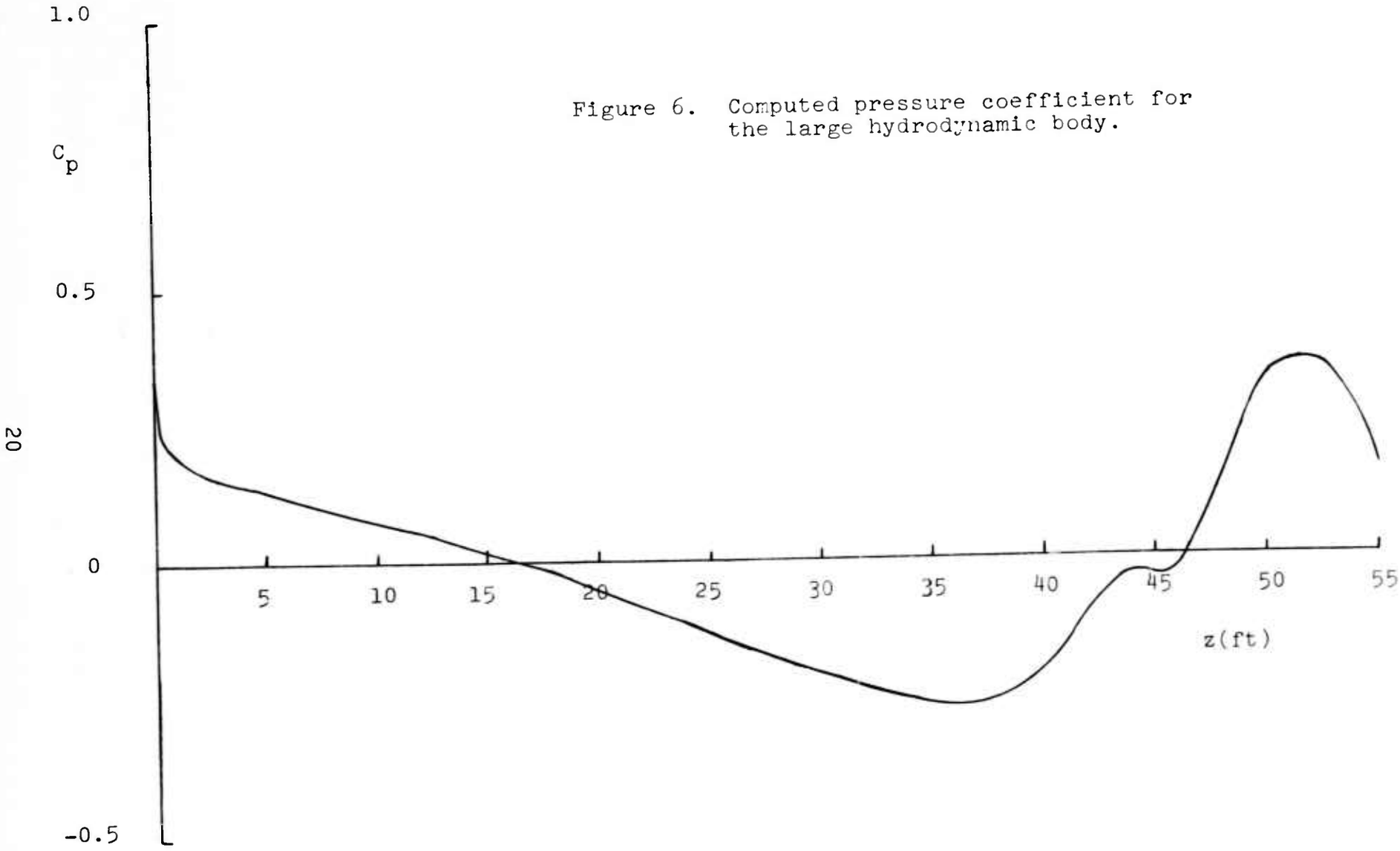

Figure 6. Computed pressure coefficient for the large hydrodynamic body.

Table 2. Computed Transition Conditions for the R-9a Body.

U_∞ (knots)	$\bar{q}_w$ ($\frac{\text{kwatts}}{\text{ft}^2}$)*	s_t (ft)	10^{-6} Re_{s_t}
30	1.40	13.9	49.1
35	2.08	11.3	46.1

*To facilitate comparison with the H-2 body heating rates, the value of $\bar{q}_w$ has been computed by integrating from s=0 to s=4 feet (see Equation 24).

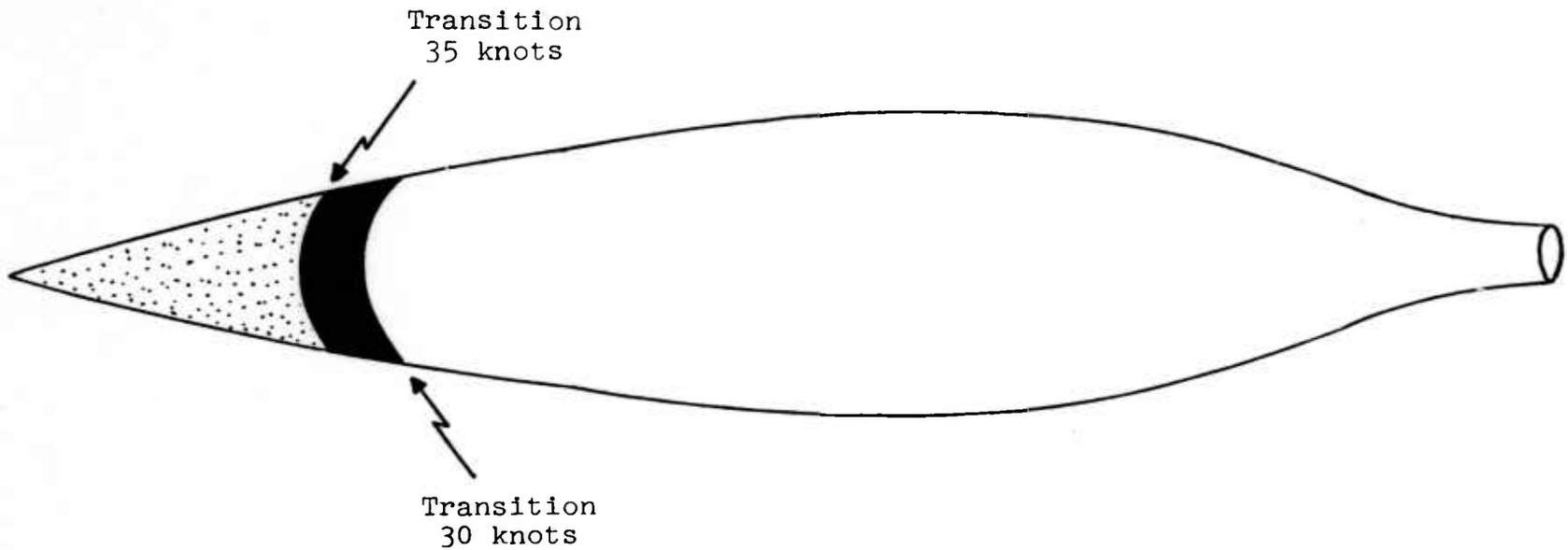

Figure 7. Computed transition location on the large hydrodynamic body.

4. SUMMARY AND CONCLUSIONS

Results reported in Section 3 demonstrate the transition model's accuracy for boundary layers with surface heat transfer, provided nonuniform viscosity effects are taken into account (Subsection 2.2). With no parameter adjustment, the model accurately predicts transition Reynolds number for (a) incompressible smooth-wall aerodynamic boundary layers with surface heating and cooling, (b) cooled rough-wall boundary layers on blunt bodies in a hypersonic air-stream, and (c) heated hydrodynamic boundary layers on small bodies.

Results of the hydrodynamic computations agree with the measured strong boundary-layer stabilization attending small amounts of surface heating. The model also predicts that large amounts of heating are not significantly more effective in delaying transition than the smaller rates considered in the H-2 body computations of Subsection 3.2. The larger R-9a body computations suppcrt this prediction.

APPENDIX A
THERMODYNAMIC PROPERTIES OF WATER

The following thermodynamic properties of water are pertinent to boundary layer transition: mass density (ρ), specific heat (C_p), thermal conductivity, (κ), molecular viscosity (μ), and laminar Prandtl number (Pr_L). Values used in this study for these quantities have been obtained from Schlichting[10] and are valid for temperatures ranging from about 40°F. to 110°F.

Mass density, specific heat, and thermal conductivity are approximately constant and have the following values:

$$\rho = 1.936 \quad \text{lbf}\cdot\text{sec}^2/\text{ft}^4 \tag{A1}$$

$$C_p = 1 \quad \text{Btu/lbf}\cdot{}^\circ\text{F} \tag{A2}$$

$$\kappa = 0.35 \quad \text{Btu/ft}\cdot\text{hr}\cdot{}^\circ\text{F} \tag{A3}$$

Viscosity and Prandtl number, by contrast, are strongly temperature dependent over this range of temperatures. An approximate polynomial fit to the Schlichting data was used to calculate μ in the computations of Section 3, i.e.,

$$\mu = 7.943\cdot10^{-6}\,(T/600)^{-8} \quad \text{lbf}\cdot\text{sec/ft}^2 \tag{A4}$$

with temperature, T, in degrees Rankine. Finally, the laminar Prandtl number follows from its definition, namely, $Pr_L=\mu C_p/\kappa$, wherefore,

$$Pr_L = 2.51(T/600)^{-8} \tag{A5}$$

Figure A1 compares Equations A4 and A5 with the measured dependences of μ and Pr_L upon temperature.

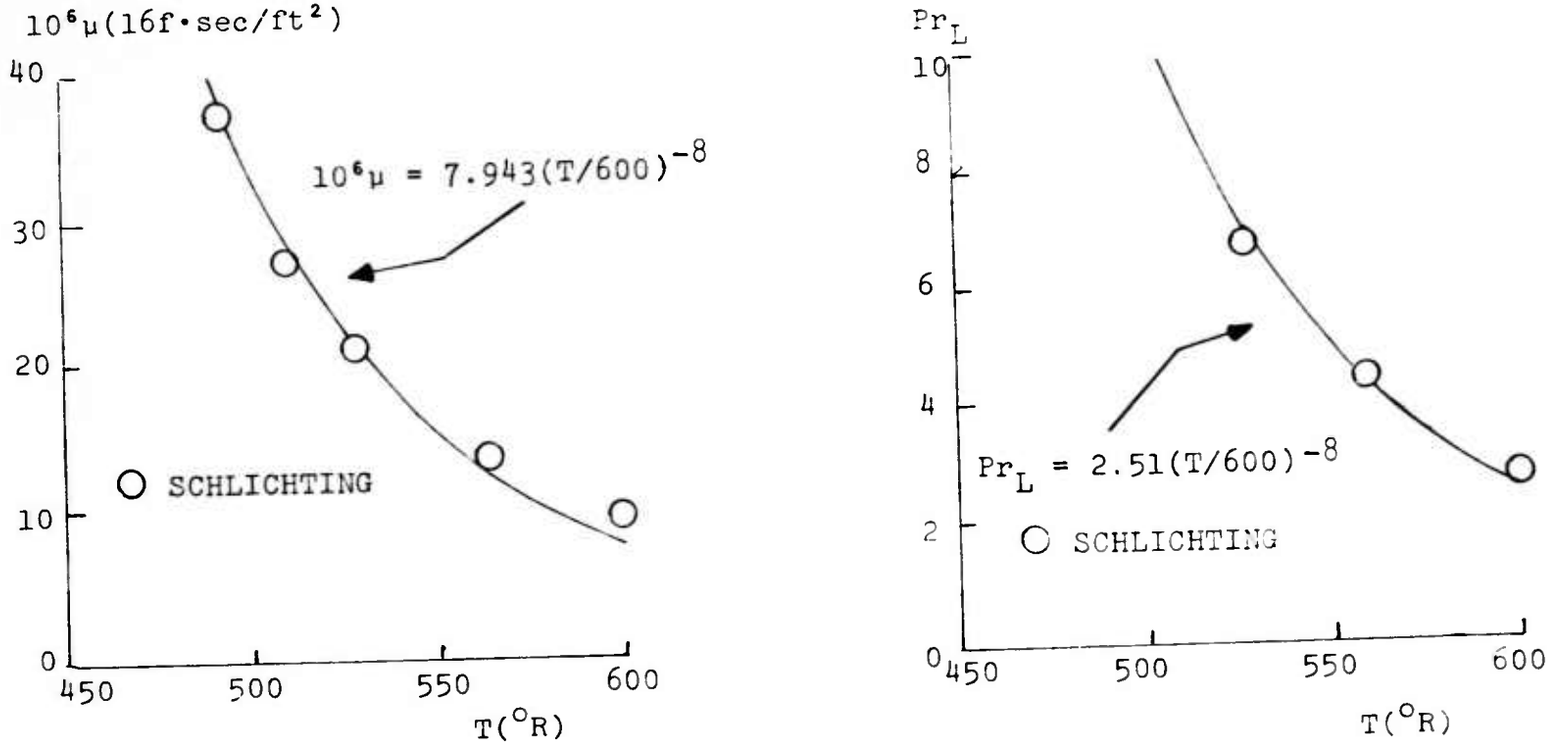

Figure A1. Molecular viscosity and laminar Prandtl number for water.

APPENDIX B
HYDRODYNAMIC BODY SHAPE PARAMETERS

The two hydrodynamic bodies analyzed in this study are specified in terms of the eight dimensionless parameters used by Parsons, Goodson, and Goldschmied[8]. The values of these parameters are as follows:

Parameter	H-2 Body	R-9a Body
f_r	4.450	5.000
x_m	0.427	0.600
k_i	2.715	4.000
r_n	0.260	0.050
r_i	0.740	0.700
s_i	1.650	1.750
x_i	0.595	0.800
t	0.180	0.150

Additionally, the H-2 body is 9.457 feet long and has a volume of 14.5 cubic feet; the R-9a body is 55 feet long and has a volume of 2500 cubic feet.

REFERENCES

1. Personal communication between D.C. Wilcox of DCW Industries and C. Gazley of the RAND Corp (May 1975).

2. Wilcox, D. C., "Turbulence-Model Transition Predictions for Blunt-Body Flows," AFOSR-TR-74-1714 (July 1974).

3. Wilcox, D.C., "Turbulence Model Transition Predictions," AIAA Journal, Vol 13, No 2, pp 241-243 (1975).

4. Wilcox, D.C. and Chambers, T.L. "Further Refinement of the Turbulence-Model Transition-Prediction Technique," DCW-R-03-02 (July 1975).

5. Shamroth, S.J. and McDonald, H., "Assessment of a Transitional Boundary Layer Theory at Low Hypersonic Mach Numbers," NASA CR-2131 (November 1972).

6. Zysina-Molozhen, L.M. and Kuznetsova, V.M., "Investigation of Turbulent Conditions in a Boundary Layer," Thermal Engineering (Teploenergetika), Vol 16, No 7, pp 16-20 (1969).

7. Anderson, A.D., "Interim Report Passive Nosetip Technology (PANT) Program, Volume 2, Summary of Experimental Results," Appendix A, Aerotherm Report 74-100 (1975).

8. Parsons, J.S., Goodson, R.E. and Goldschmied, F.R., "Shaping of Axisymmetric Bodies for Minimum Drag in Incompressible Flow," Journal of Hydronautics, Vol 8, No 3 (July 1974).

9. Smith, A.M.O. and Pierce, J., "Exact Solution of the Neumann Problem. Calculation of Non-Circulatory Plane and Axially Symmetric Flows about or within Arbitrary Boundaries," Report ES26988, Douglas Aircraft Co, Long Beach, CA (April 1958).

10. Schlichting, H., Boundary Layer Theory, Fourth Edition, McGraw-Hill, p 8 and p 294 (1960).

DISTRIBUTION

Air Force Office of Scientific Research
1400 Wilson Blvd.
Arlington, Virginia 22209

Prototype Development Associates, Inc.
1740 Garry Avenue, Suite 201
Santa Ana, California 92705
Attn: J. Dunn

Jet Propulsion Laboratory
Gas Dynamics Section
4800 Oak Grove Drive
Pasadena, California 91109
Attn: J. Kendall
L. Mack

University of Southern California
Dept. of Aerospace Engineering
University Park
Los Angeles, California 90007
Attn: J. Laufer

Lockheed Missiles & Space Co.
Continental Building, Suite 445
101 Continental Blvd.
El Segundo, California 90245
Attn: T. Fortune

AEDC
AFSC, USAF
Arnold Air Force Station
Tennessee 97389
Attn: J. Miller

Flow Research, Inc.
5959 West Century Boulevard, Suite 912
Los Angeles, California 90045
Attn: D. Ko

Calspan Corporation
P.O. Box 235
Buffalo, New York 14221
Attn: M. Holden

Philco-Ford Corporation
Space & Reentry Systems
Ford Road
Newport Beach, California 92663
Attn: A. Demetriades
C. White

Avco Corporation
201 Lowell Street
Wilmington, Massachusetts 01887
Attn: A. Pallone
V. DiCristina

General Electric
3198 Chestnut Street
Philadelphia, Pennsylvania 19101
Attn: A. Martellucci

McDonnell-Douglas Corporation
5301 Bolsa Avenue
Huntington Beach, California 92647
Attn: K. Kratsch

Physical Sciences, Inc.
18 Lakeside Office Park
Wakefield, Massachusetts 01880
Attn: M. Finson

Director of Defense Research and
Engineering (Strategic Weapons)
The Pentagon
Washington, D.C. 20330
Attn: R. Ruffine

Department of Aerospace & Mechanical
Engineering Sciences
University of California
P.O. Box 109
La Jolla, California 92038
Attn: S. Penner

Defense Documentation Center
Cameron Station
Alexandria, Virginia 22314

Applied Physics Laboratories
Johns Hopkins University
Silver Spring, Maryland 20390
Attn: Dr. Stone

Defense Advanced Research Projects
Agency
1400 Wilson Boulevard
Arlington, Virginia 22209
Attn: TIO
K. Kresa
R. Moore

Air University Library
Maxwell Air Force Base
Alabama 36112
Attn: AUL 3T-64-316

Acurex Corporation
485 Clyde Avenue
Mountain View, California 94040
Attn: R. Kendall
R. Rindal

DISTRIBUTION (continued)

Avco Everett Research Laboratory
2385 Revere Beach Parkway
Everett, Massachusetts 02149
Attn: K. Wray

Boeing Company
Seattle, Washington 98124
Attn: R. Montgomery

Battelle Memorial Institute
505 King Avenue
Columbus, Ohio 43201
Attn: Defender (E. Unger)

Commanding Officer
Ballistics Research Laboratories
Aberdeen Proving Ground, Maryland 21005
Attn: C. Murphy

Arnold Engineering Development Center
Von Karman Gas Dynamics Facility
Tullahoma, Tennessee 37389
Attn: J. Hahn

Office of Naval Research
Department of the Navy
Washington, D.C. 20360
Attn: Phys, Br. (Code 421)
Dr. Isakson

TRW Systems, Inc.
One Space Park
Redondo Beach, California 92078
Attn: L. Hromas

U.S. Army Advanced Ballistic Missile
Defense Agency
Commonwealth Building
1320 Wilson Boulevard
Arlington, Virginia 22209
Attn: CRDABM-RD (Street G)
RP (Rep)
DT (Rep)

Massachusetts Institute of Technology
Lincoln Laboratory
244 Wood Street
Lexington, Massachusetts 02173
Attn: BMRS Project

NASA Scientific & Technical Information
Facility
P.O. Box 33
College Page, Maryland 20740
Attn: Acquisitions BR(S-AK-DL)

California Institute of Technology
Pasadena, California 91109
Attn: L. Lees
H. Liepmann
P. Saffman

Arnold Engineering Development Center
Tullahoma, Tennessee 97389
Attn: J. Miller

AF Cambridge Research Laboratory
Lawrence G. Hanscom Field
Bedford, Massachusetts 01730
Attn: CRMXLR, STOP 29

Air Force Flight Dynamics Laboratory
Wright-Patterson Air Force Base
Ohio 45433
Attn: M. Buck
W. Hankey
J. Shang
P. Knight

Air Force Materials Laboratory
Wright-Patterson Air Force Base
Ohio 45433
Attn: G. Jumper
K. Stetson

Air Force Weapons Laboratory
Kirtland Air Force Base
Albuquerque, New Mexico 87115
Attn: WLRA/Capt. Koziol
J. Ortwerth

Commanding General
U.S. Army Safeguard Systems Command
P.O. Box 1500
Huntsville, Alabama 35807
Attn: SENSC-Y

U.S. Naval Surface Weapons Center
White Oak, Silver Springs, Maryland 20910
Attn: Librarian
D. Reda
C. Lyons
R. Phinney

Institute for Defense Analysis
Science and Technology Division
400 Army-Navy Drive
Arlington, Virginia 22202
Attn: H. Liepmann

DISTRIBUTION (continued)

Case Western Reserve University
Cleveland, Ohio
Attn: E. Reshotko

NASA Langley Research Center
Hampton, Virginia 23665
Attn: I. Beckwith
J. Harris
D. Bushnell
C. Anderson

RAND Corporation
1700 Main Street
Santa Monica, California 90406
Attn: C. Gazley

NASA Ames Research Center
Moffett Field, California 94035
Attn: M. Rubesin
J. Marvin
B. Baldwin

Space & Missile Systems Organization
P.O. Box 92960
Worldway Postal Center
Los Angeles, California 90009
Attn: T. Hopkins
E. Taylor

The Aerospace Corporation
P.O. Box 92957
Los Angeles, California 90009
Attn: W. Portenier

Naval Underwater Systems Center
Newport, Rhode Island 02840
Attn: G. Christoph

Lawrence Livermore Laboratories
P.O. Box 808
Livermore, California 94550
Attn: A. Buckingham

DCAS
14450 Erwin Street
Van Nuys, California 91408
Attn: H. Moses

U.S. Naval Weapons Laboratory
Dahlgren, Virginia 22448
Attn: Code KRT (MODE)

Los Alamos Scientific Laboratory
Group T-3, Mail Stop 216
P.O. Box 1663
Los Alamos, New Mexico 87544
Attn: J. Ramshaw

University of California, Berkeley
College of Engineering
Berkeley, California 94720
Attn: S. Berger

Stanford University
Department of Mechanical Engineering
Palo Alto, California 94305
Attn: W. Reynolds

UNCLASSIFIED

SECURITY CLASSIFICATION OF THIS PAGE (When Data Entered)

REPORT DOCUMENTATION PAGE		READ INSTRUCTIONS BEFORE COMPLETING FORM
1. REPORT NUMBER AFOSR-TR-75-1398	2. GOVT ACCESSION NO. ADA015938	3. RECIPIENT'S CATALOG NUMBER AD-A107 624
4. TITLE (and Subtitle) EFFECTS OF SURFACE HEAT TRANSFER ON BOUNDARY-LAYER TRANSITION		5. TYPE OF REPORT & PERIOD COVERED INTERIM 1 April-30 July 1975 6. PERFORMING ORG. REPORT NUMBER DCW-R-03-03
7. AUTHOR(s) DAVID C. WILCOX THOMAS L. CHAMBERS		8. CONTRACT OR GRANT NUMBER(s) F44620-74-C-0048
9. PERFORMING ORGANIZATION NAME AND ADDRESS DCW INDUSTRIES 13535 VENTURA BOULEVARD, SUITE 207 SHERMAN OAKS, CALIFORNIA 91423		10. PROGRAM ELEMENT, PROJECT, TASK AREA & WORK UNIT NUMBERS 681307 9781-02 61102F
11. CONTROLLING OFFICE NAME AND ADDRESS AIR FORCE OFFICE OF SCIENTIFIC RESEARCH/NA 1400 WILSON BOULEVARD ARLINGTON, VIRGINIA 22209		12. REPORT DATE July 1975 13. NUMBER OF PAGES 37
14. MONITORING AGENCY NAME & ADDRESS(if different from Controlling Office)		15. SECURITY CLASS. (of this report) UNCLASSIFIED 15a. DECLASSIFICATION/DOWNGRADING SCHEDULE

16. DISTRIBUTION STATEMENT (of this Report)

Approved for public release; distribution unlimited.

17. DISTRIBUTION STATEMENT (of the abstract entered in Block 20, if different from Report)

18. SUPPLEMENTARY NOTES

19. KEY WORDS (Continue on reverse side if necessary and identify by block number)

BOUNDARY LAYER TRANSITION
TURBULENCE PREDICTION
TRANSITION PREDICTION
BLUNT-BODY FLOWS
SURFACE HEATING

20. ABSTRACT (Continue on reverse side if necessary and identify by block number)

Effects of surface heat transfer on boundary-layer transition are analyzed in a three-part study using the Saffman-Wilcox transition model. In the first part of the study, model predictions are compared with experimental data for cooled and heated aerodynamic boundary layers on smooth flat surfaces and for cooled aerodynamic boundary layers near the stagnation point of a roughened blunt body. Consistent with measurements, the model predicts, on the one

DD FORM 1 JAN 73 1473 EDITION OF 1 NOV 65 IS OBSOLETE

UNCLASSIFIED

SECURITY CLASSIFICATION OF THIS PAGE (When Data Entered)

hand, that heating destabilizes a smooth-surface aerodynamic boundary layer and, on the other hand, that cooling destabilizes a rough-surface aerodynamic boundary layer. Differences between predicted and measured transition-point locations are within experimental error bounds. Then, incipient transition conditions are determined for a small, heated hydrodynamic body. Again model predictions agree with measurements which indicate that relatively small amounts of surface heating have a strong stabilizing effect on hydrodynamic boundary layers. In the final part of the study, transition location is determined for a large hydrodynamic body; results indicate that large surface heating rates are not substantially more effective than smaller rates.